IEEE Access
Multidisciplinary | Rapid Review | Open Access Journal

Date of publication xxxx 00, 0000, date of current version xxxx 00, 0000.

Digital Object Identifier 10.1109/ACCESS.2022.0122113

End-to-end Performance Evaluation of SLP Waveforms

JEVGENIJ KRIVOCHIZA, (Member, IEEE), JUAN DUNCAN, (Senior Member, IEEE), JORGE QUEROL, (Member, IEEE), and SYMEON CHATZINOTAS, (Fellow Member, IEEE)
[1]University of Luxembourg, SnT, 29 Avenue JF Kennedy, L-1855 Luxembourg (e-mail: jevgenij.krivochiza@uni.lu)
Corresponding author: Jevgenij Krivochiza (e-mail: jevgenij.krivochiza@uni.lu).

This research was funded in whole, or in part, by the Luxembourg National Research Fund (FNR), grant reference [IPBG19/14016225/INSTRUCT].

ABSTRACT In this paper, we investigate the demodulation and decoding of the symbol-level precoded (SLP) signal using the conventional logarithmic likelihood ratio (LLR) and low-density parity check (LDPC) decoding algorithms operating in real-time on the software-defined radio (SDR) receiver. Its conventional forward error correction (FEC) was designed assuming symmetric additive white Gaussian noise (AWGN). While SLP generates asymmetric constellation point clouds it is unclear if it can achieve similar FEC gains in an end-to-end coded setup. The receiver is implemented based on the DVB-S2X standard. It estimates multi-beam interference-limited channel coefficients by using the orthogonal pilots embedded into the DVB-S2X frames to facilitate precoding at the transmitter. After the received frames are fully synchronized the payload symbols are decoded in two stages: soft decision using the LLR and hard decision using the LDPC decoders. We benchmark the bit error rate (BER) and frame error rate (FER) of the complete decoding chain while using the zero-forcing (ZF) and the selected SLP channel-interference canceling techniques. The conducted in-lab experiments show that the SLP can improve BER and FER performance in the conventional receiving and decoding design for symmetric constellations while achieving its original optimization goals.

INDEX TERMS Satellite communication, Non-terrestrial networks, User terminals, Precoding, Interference cancellation

I. INTRODUCTION

Terrestrial and satellite communications (SATCOMs) are an integral part of the future technologies and use cases proposed by the telecommunication industry [1]. The global broadband access demand is rising together with the demand for high-speed internet connectivity, facilitated by the global digitization of all private and state sectors. 5G non-terrestrial networks (NTN) [2] can provide connected services to remote areas and complement the terrestrial services [3].

In this scope, we focus on the multi-beam high-throughout satellites and the full frequency reuse (FFR) approach to achieve maximum throughput and spectrum efficiency. Both DVB-S2X [4] and 5G communications standards allow FFR to be implemented. Recent works study the practical application of precoding in SATCOM to cancel the interference in FFR scenarios [5]–[7]. Precoding is implemented at the gateway in the digital domain [8]. In recent years, many extensive in-lab and field tests were published to increase technology readiness level (TRL) and demonstrate precoding benefits in SATCOMs [9]–[11]. In [12]–[14] the authors presented an in-lab real-time satellite precoded transmission test-bed, where a satellite has 6 transmitting antennas and simultaneously serves 6 user terminals (UTs). The demonstrated test bed was developed for the in-lab environment and tested over the simulated multi-beam satellite channel. The authors in [15] and [16] showcased over-the-air validations using actual satellite links by using closed-loop precoding. The authors in [17] demonstrated their field trials of multi-satellite multi-user precoding. Linear precoding was experimentally verified over the actual satellite link in [18] using the standard DVB-S2X framing.

The conventional channel-based precoding techniques use the knowledge of channel state information (CSI) to generate the optimal precoder. The most common channel-based strategies are zero-forcing (ZF) and the minimal means square error (MMSE) precoding methods [19]–[21]. Advanced precoding techniques, such as symbol-level precoding (SLP), use the CSI and calculate the optimal precoder for each individual transmitted data symbol to achieve more power-efficient signaling and service availability [22]. Despite numerous publications on SLP techniques, the effect of per-symbol optimizations by SLP on end-to-end coding and decoding performance remains unclear. Conventional forward error correction (FEC) was designed assuming symmetric Additive White Gaussian Noise (AWGN). Contrariwise to this assumption, SLP generates asymmetric constellation point clouds. It is unclear if the theoretical FEC gains are maintained in an end-to-end coded setup.

In this paper, we investigate the demodulation and decoding of SLP symbols in the conventional LDPC and LLR-based receiver. The preliminary results and broader discussions on SLP decoding were presented in the Ph.D. thesis by the corresponding author [23]. Here, we focus on the performances of the coded BER and FER and the spectral efficiency of the receiver running in real-time operation mode. The implemented DVB-S2X compatible receiver is based on the software-defined radio (SDR) technology, equipped with the industry-standard FEC. The receiver estimates SINR from the pilots embedded into the DVB-S2X frame and decodes information bits from the data symbols using logarithmic likelihood ratio (LLR) estimations and the low-density parity check (LDPC) decoder. We compare the SINR, BER, FER, and spectral efficiency performance of SLP to a conventional ZF precoding technique to evaluate the receiver's performance. In this benchmark, the receiver was not modified to decode symbols enhanced by the SLP processing at the transmitter side. Thus, we investigate the impact of the SLP symbols on a conventional receiver chain. The benchmark resembles a realistic SLP processing deployment in a communication system, where only the transmitter is modified, while the user terminals remain unchanged.

II. SYSTEM DESCRIPTION

A. SYSTEM MODEL

We consider a system model with the forward link of a multi-user multi-antenna wireless communication system. We assume the system to use the full frequency reuse scenario, in which all the antennas transmit in the same frequency and time domains. The multi-user interference is managed using precoding. We define the number of the transmitting antennas as N_t and the total number of single-antenna UTs as N_u in the coverage area. In the specified MU-MIMO channel model, the received signal at the i-th UT is given by $y_i = \mathbf{h}_i^\dagger \mathbf{x} + u_i + n_i$, where $\mathbf{h}_i^\dagger$ is a $1 \times N_t$ vector representing the complex channel coefficients between the i-th UT and the N_t antennas of the transmitter, $\mathbf{x}$ is defined as the $N_t \times 1$ vector of the transmitted symbols at a certain symbol period, u_i is a constructive interference component of SLP precoding, and n_i is the independent complex circular symmetric (c.c.s.) independent identically distributed (i.i.d) zero mean AWGN measured at the i-th terminal's receive antenna.

Looking at the concatenated formulation of the received signal, which includes the whole set of receiver terminals, the linear signal model is

$$\mathbf{y} = \mathbf{H}\mathbf{x} + \mathbf{u} + \mathbf{n} = \mathbf{H}\mathbf{W}(\mathbf{s} + \mathbf{u}) + \mathbf{n}, \tag{1}$$

where $\mathbf{y} = [y_1, y_i, \ldots, y_{N_u}] \in \mathbb{C}^{N_u \times 1}$, $\mathbf{n} = [n_1, n_i, \ldots, n_{N_u}] \in \mathbb{C}^{N_u \times 1}$, $\mathbf{x} \in \mathbb{C}^{N_t \times 1}$, $\mathbf{s} \in \mathbb{C}^{N_u \times 1}$, $\mathbf{u} = [u_1, u_i, \ldots, u_{N_u}] \in \mathbb{C}^{N_u \times 1}$ and $\mathbf{H} = [\mathbf{h}_1^\dagger, \mathbf{h}_i^\dagger, \ldots, \mathbf{h}_{N_u}^\dagger] \in \mathbb{C}^{N_u \times N_t}$. We define a precoding matrix $\mathbf{W} \in \mathbb{C}^{N_t \times N_u}$ which maps the information symbols $\mathbf{s}$ into precoded symbols $\mathbf{x}$. We consider the data symbols $\mathbf{s}$ to be unit variance complex vectors $|s_i| = 1$ for every $i = 1, 2, \ldots, N_u$. The vector $\mathbf{u}$ represents the constructive interference in the received symbols of all the users. The precoding matrix $\mathbf{W}$ and the vector $\mathbf{u}$ are defined according to the selected precoding technique, which we describe in the following section.

B. PRECODING TECHNIQUES

1) Channel Inversion

We define the precoding matrix $\mathbf{W}_{ZF}$ as the ZF precoder:

$$\mathbf{W}_{ZF} = \mathbf{H}^H(\mathbf{H}\mathbf{H}^H)^{-1}/f_{ZF}, \tag{2}$$

where $f_{ZF} = \sqrt{\sum_{n=1}^{N_t}\sum_{m=1}^{N_u} \mathbf{W}_{ZF_{n,m}}^2}$ is a rescaling factor to account for sum power constraints. In this case $u_i = 0$ for all $i = 1, 2, \ldots, N_u$.

2) Symbol-Level Precoding

We define the SLP as in [22]. This SLP aims to minimize the total transmitted power while respecting SINR constraints at the terminals. The technique is not targeting to improve SINR at the receivers, but can introduce constructive interference to the received symbols. We chose the SLP technique for its low complexity, which was optimized to run in real-time transmission mode using field-programmable gate array (FPGA) acceleration. The SLP technique solves a convex optimization problem for the N_u terminals to jointly optimize the transmitted modulated signals on the N_t antennas. The following optimization problem is devoted:

$$\begin{aligned} \min_{\mathbf{u}} \quad & \|\mathbf{W}_{ZF}\mathbf{B}(\tilde{\mathbf{s}} + \tilde{\mathbf{u}})\|_2 \\ \text{s.t.} \quad & \tilde{u}_i \geq 0, \end{aligned} \tag{3}$$

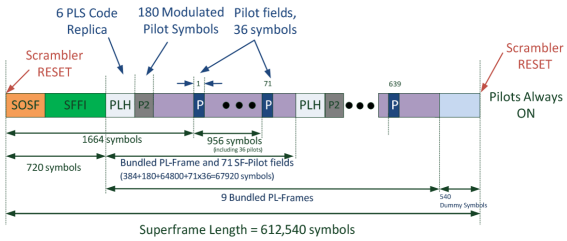

FIGURE 1. Stucture of DVB-S2X frame [26].

where $\tilde{u}_i$ is the constructive interference for the symbol $\tilde{s}_i = 1$ for every $i = 1, 2, \ldots, N_u$ and $\mathbf{B}$ is the rotation matrix of the symbol vectors and is defined as

$$\mathbf{B} = \begin{bmatrix} s_1 & 0 & 0 & \ldots & 0 \\ 0 & s_2 & 0 & \ldots & 0 \\ 0 & 0 & s_i & \ldots & 0 \\ \vdots & \vdots & \vdots & \ddots & \vdots \\ 0 & \ldots & 0 & 0 & s_{N_u} \end{bmatrix}. \tag{4}$$

The following equality is therefore respected

$$\mathbf{s} = \mathbf{B}\tilde{\mathbf{s}}. \tag{5}$$

.

The problem (3) is a non-negative least squares (NNLS) problem. It can be solved directly by using the Fast NNLS algorithm developed in [24]. In [25] we proposed the closed-form sub-optimal solution as follows

$$\tilde{\mathbf{u}} = \text{diag}[(\widetilde{\mathbf{A}}^T\widetilde{\mathbf{A}})^{-1}]\widetilde{\mathbf{A}}^T\tilde{\mathbf{d}}. \tag{6}$$

where $\widetilde{\mathbf{A}} = [\text{Re}(\mathbf{A}); \text{Im}(\mathbf{A})]$, $\tilde{\mathbf{d}} = [\text{Re}(\mathbf{d}^T), \text{Im}(\mathbf{d}^T)]^T$, $\mathbf{A} = \mathbf{W}_{ZF}\mathbf{B}$ and $\mathbf{d} = -\mathbf{W}_{ZF}\mathbf{B}\tilde{\mathbf{s}}$. We do not show the complete derivation steps to get this solution as it is out of the scope of this paper. In [22] it was demonstrated that this algorithm provides a good trade-off between the precision of the results and the real-time performance capabilities using the FPGA acceleration.

Further in the paper, we will refer to the SLP technique based on the convex problem (3) and solved by closed-form algorithm (6) as CF NNLS SLP.

C. DATA-AIDED CHANNEL ESTIMATION

The UTs use the pilots of the superframe format 2 (Fig. 1) to estimate CSI.

The pilot k-th sequence P_k is generated as in [26]. The pilot fields are determined by a WH sequence of size 32 symbols. The pilot sequences are transmitted as BSPK modulated symbols by applying $(1+\iota)\sqrt{2}$ to each element of the sequences. Each user knows its dedicated sequence k.

We can distinguish each orthogonal WH sequence in the jointly received signal and estimate CSI for the k-th received signal at the i-th UT side as

$$CSI_{i,k} = \sum_{t=1}^{32} y_i[t] \times P_k[t]. \tag{7}$$

The estimated channel matrix is then formed at the transmitter based on the reported CSI as

$$\widetilde{\mathbf{H}} = \begin{bmatrix} CSI_{1,1} & CSI_{1,2} & \ldots & CSI_{1,N_t} \\ CSI_{2,1} & CSI_{2,2} & \ldots & CSI_{2,N_t} \\ \vdots & \vdots & \ddots & \vdots \\ CSI_{N_u,1} & CSI_{N_u,2} & \ldots & CSI_{N_u,N_t} \end{bmatrix}. \tag{8}$$

D. DATA-AIDED SINR ESTIMATION

To evaluate the performance of the precoding techniques, we consider the signal-to-interference-plus-noise ratio (SINR) by measuring the actual pilots at the UT side rather than using SINR estimation based on the precoding matrix [27]. SINR estimation is suitable for SLP techniques, where SINR depends on both the precoding matrix and the symbol constructive interference. We use the signal-to-noise ratio estimation (SNORE) algorithm [28].

In data-aided (DA) mode, the SNORE algorithm uses the pilot signals that are present in the transmitted frames. The pilots are used to estimate the SINR of the payload symbols, which are precoded with the same technique as the pilots. The pilots are based on a known bit sequence (P2) and modulated with BSPK, as described in [26]. The DVB-S2X standard follows this method and sends pilots at the start of each frame for each user.

At each UT, the SINR is calculated as follows:

$$\frac{E_b}{N_0} = \frac{P_s}{P_n}, \tag{9}$$

where P_s - power of the intended signal and P_N - power of noise plus interference. We calculate P_s as

$$P_s = |\frac{1}{180}\sum_{t=1}^{180} y_i[t] \times P2[t]|^2 \tag{10}$$

We calculate P_N from the total signal power

$$P_n = P_r - P_s, \tag{11}$$

where $P_r = \frac{1}{180}\sum_{t=1}^{180} |y_i[t]|^2$.

E. LLR CALCULATION

To deal with the noisy channels the UTs apply FEC to demodulate symbols and to improve the communication quality. They use the LLR algorithm for soft demodulation and get the LLR values for the LDPC decoder. The

TABLE 1. LDPC decoder supported modes.

Mode	Frame Size	Code rate (C_R)
1	64800	1/2
2	64800	2/3
3	64800	3/4
4	64800	5/6

decoder uses these values to recover the information bits from the symbols. The LLR is given by:

$$\mathrm{LLR_j} = \ln\left[\frac{\sum_{\mathrm{b:b_j=0}} \exp\left(\frac{-|\mathrm{y_i[t]-c(b)}|^2}{2\sigma^2}\right)}{\sum_{\mathrm{b:b_j=1}} \exp\left(\frac{-|\mathrm{y_i[t]-c(b)}|^2}{2\sigma^2}\right)}\right], \qquad (12)$$

where $\mathrm{y_i[t]}$ is the received complex symbol, c is the nominal constellation complex point, and σ^2 is the noise variance. To calculate the LLR of the j-th bit from $\mathrm{y_i[t]}$, we compute the squared distance between $\mathrm{y_i[t]}$ and each constellation point, and separate them by their j-th bit value. A common simplification of the LLR is to use only the closest constellation point with $\mathrm{b_j} = 0$ in the numerator and the closest one with $\mathrm{b_j} = 1$ in the denominator. The simplified LLR is:

$$\mathrm{LLR_j} = \frac{1}{2\sigma^2}\left(|\mathrm{y_i[t]} - \mathrm{c_1}|^2 - |\mathrm{y_i[t]} - \mathrm{c_0}|^2\right), \qquad (13)$$

as shown in [13]. We use equation (13) in the following benchmarks.

F. LDPC DECODER

The FEC system can correct more errors if it has more redundancy and a better coding algorithm. The LDPC codes are very good channel codes that can achieve near-optimal error correction. They also allow efficient hardware architectures because they can be processed in parallel. The LDPC decoder in the receiver uses the LDPC Block Codes (LDPC-BC) or QC-LDPC Quasi-Cyclic LDPC Codes, as the DVB-S2 standard specifies [26], [28]. These LDPC codes have block-structured LDPC codes with circular block matrices. The whole parity check matrix can be divided into smaller block matrices, which are either zero matrices or right cyclic shifts of identity matrices. The parity check matrix can be represented by a base matrix with cyclic shifts. This feature has the advantage of providing high throughput and low complexity in implementation. The current LDPC decoder implementation uses a log-domain LDPC iterative decoding algorithm (Belief propagation) approximation called the layered offset min-sum algorithm [29].

The supported modes of the UT LDPC decoder are presented in Table 1.

III. EXPERIMENTAL VALIDATION

A. IN-LAB VERIFICATION STAND

For the experimental validation, we built the in-lab verification stand. It consists of the multi-antenna transmitter, the channel emulator, and the UTs. The RF hardware is based on the National Instruments SDRs. Each SDR has 2 RF inputs and 2 RF outputs operating in the full duplex mode.

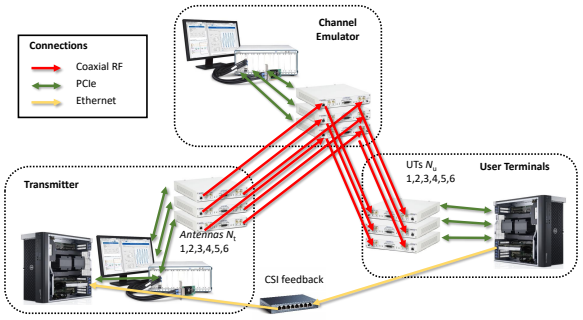

FIGURE 2. Precoding validation demo.

As shown in Fig. 2 the transmitter simultaneously transmits 6 precoded signals towards 6 UTs through a 6-by-6 multi-beam satellite channel emulator. The channel emulator acquires the gateway signals, applies Gaussian noise and multi-beam interference, and transmits the signals to the UTs. The UTs estimate the CSI based on the DVB-S2X pilots and report the estimated values to the gateway through a dedicated feedback channel over an Ethernet link. This setup allows us to test the receivers in real-time operation mode while using actual RF-modulated signals. In this setup, we provide the multi-beam interference through the emulated channel matrix, which is fixed for all the tests. When we need to change the SNR, we increase or decrease the amplitude of the Gaussian noise generator. We did not consider any other satellite channel impairments in this paper, such as payload non-linearities, phase noise, Doppler spread and shift, or timing errors, as they would further affect the SNR experienced by the UTs.

B. EMULATED CHANNEL DESCRIPTION

We use the realistic channel matrix generated based on the provided satellite beam pattern as shown in Fig. 3. In Table 2 we show the channel matrix coefficients loaded into our channel emulator [30] during the experimental validations. We have 6 transmitting antennas for each of the beams and 6 UTs located in the coverage area of at least one of the beams. Each UT is experiencing interference from the adjacent beams, which can be seen in the channel estimations reported in Table 3. The UTs estimate CSI as in (9).

The CSI is different from the actual channel matrix applied in the channel emulator due to the hardware impairments, the fixed-point implementation precision, and the cable losses between the transmitter and the UTs.

We visualize the estimated channel matrix in Fig.

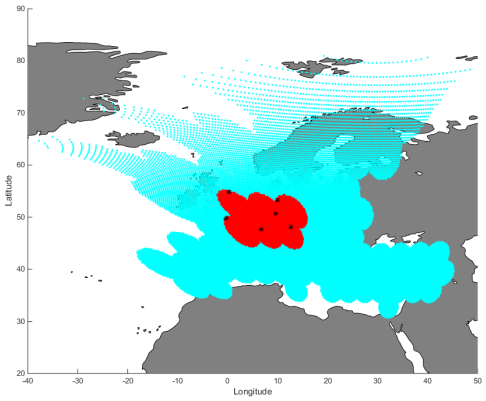

FIGURE 3. Channel selected beams configuration.

TABLE 2. Applied channel matrix in the channel emulator.

$0.2721 + 0.0000i$	$-0.0082 + 0.1513i$	$0.0052 - 0.0020i$	$-0.0154 - 0.0303i$	$-0.0075 + 0.0001i$	$-0.0067 + 0.0051i$
$-0.0172 + 0.0328i$	$0.3988 - 0.0000i$	$0.0190 + 0.0248i$	$0.0111 + 0.0037i$	$0.0515 - 0.0367i$	$0.0034 - 0.0182i$
$-0.0046 + 0.0062i$	$-0.0245 - 0.0505i$	$0.3698 + 0.0000i$	$0.00061 + 0.00085i$	$0.1573 + 0.0663i$	$0.0281 - 0.0134i$
$0.1548 + 0.0064i$	$-0.1847 + 0.0419i$	$-0.0121 + 0.0207i$	$0.2847 + 0.0000i$	$-0.0051 - 0.0320i$	$0.0184 + 0.0007i$
$0.0009 - 0.0075i$	$-0.0595 - 0.1018i$	$0.1466 - 0.0063i$	$0.0742 - 0.0377i$	$0.3857 - 0.0000i$	$0.1308 + 0.1546i$
$-0.00033 - 0.00015i$	$0.0006 + 0.0087i$	$0.2330 + 0.0942i$	$0.0003 + 0.0024i$	$-0.1504 + 0.1480i$	$0.2881 + 0.0000i$

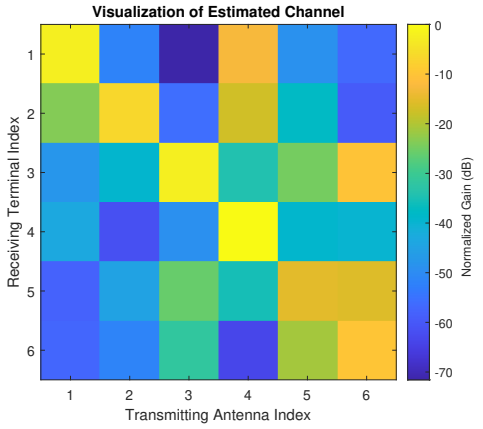

FIGURE 4. Graphical Visualisation of the Estimated Channel Matrix.

4. The visualization would look like a diagonal matrix without interference between the beams. In our case, we can see that most of the UTs experience a very strong interference. However, UT 1 has interference only from a single neighboring beam and the UT 4 has no interference at all. The UT 5 receives a very strong interference, which is as strong as its main signal carrier.

Finally, we run numerical benchmarks to estimate the performance of the precoding techniques with the

TABLE 3. Estimated channel matrix.

$0.3834 + 0.0000i$	$-0.0004 - 0.0325i$	$-0.0045 + 0.0112i$	$-0.0991 - 0.2055i$	$-0.0111 - 0.0359i$	$0.0201 - 0.0157i$
$0.0944 - 0.0920i$	$0.3101 + 0.0000i$	$0.0165 - 0.0210i$	$-0.0631 + 0.1730i$	$0.0540 + 0.0380i$	$0.0051 + 0.0216i$
$-0.0111 - 0.0383i$	$0.0382 - 0.0468i$	$0.3826 + 0.0000i$	$0.0074 + 0.0773i$	$-0.0616 + 0.1089i$	$0.0638 - 0.2535i$
$0.0470 + 0.0161i$	$-0.0164 + 0.0109i$	$-0.0369 + 0.0037i$	$0.4325 - 0.0000i$	$0.0600 - 0.0117i$	$0.0226 + 0.0545i$
$-0.0082 + 0.0223i$	$-0.0455 + 0.0045i$	$-0.1172 - 0.0148i$	$0.0079 - 0.0737i$	$0.2022 + 0.0000i$	$0.0483 + 0.1917i$
$0.0126 - 0.0213i$	$0.0325 - 0.0046i$	$0.0886 - 0.0069i$	$-0.0002 + 0.0179i$	$-0.1229 + 0.0879i$	$0.2641 + 0.0000i$

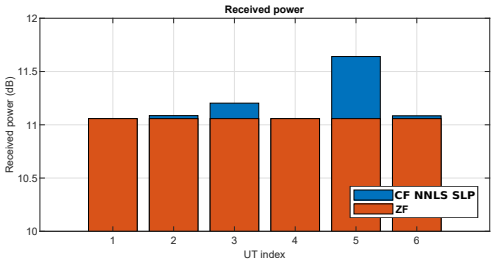

FIGURE 5. RX power at the UTs using different precoding techniques.

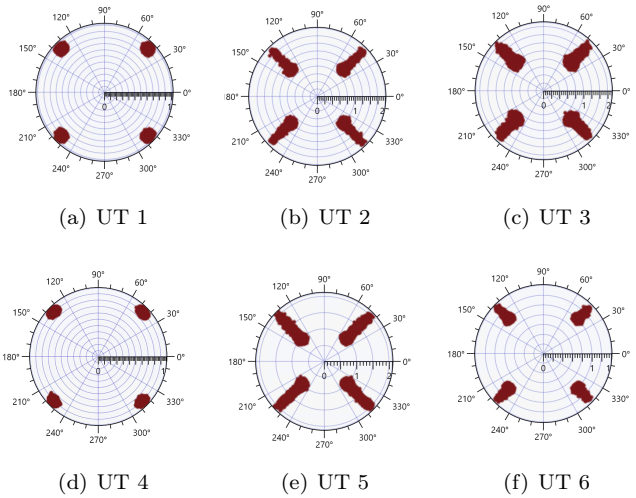

(a) UT 1 (b) UT 2 (c) UT 3

(d) UT 4 (e) UT 5 (f) UT 6

FIGURE 6. Received data QPSK symbols at UTs modified by CF NNLS SLP.

generated channel matrix. In Fig. 5 we can see the expected received power per each UT for the ZF and the SLP techniques. The SLP technique provides the gains to the UTs 2, 3, 5, and 6. It is evident, that the UT 5 has more gains due to more constructive interference preserved in the signal. UTs 1 and 4 have no visible gains due to the lack of any constructive interference at their location.

C. RECEIVED SYMBOLS OF SLP

In Fig. 6 we can see the received QPSK symbols for each UT. The BF symbols modified by the SLP are visible in UTs 2, 3, 5, and 6. These results match the theoretically predicted gains derived from the channel matrix analysis.

D. SINR PERFORMANCE OF CF NNLS SLP

We focus on UT 5 as it is the one most affected by the SLP technique. We set the relative noise power in the channel emulator to 0 to measure the SINR (SINR_0) at the UT for the ZF technique. We then increase the relative noise power with a 0.2 dB step to measure the SINR estimations in the region of our interest. We calculate the average SINR value and the standard

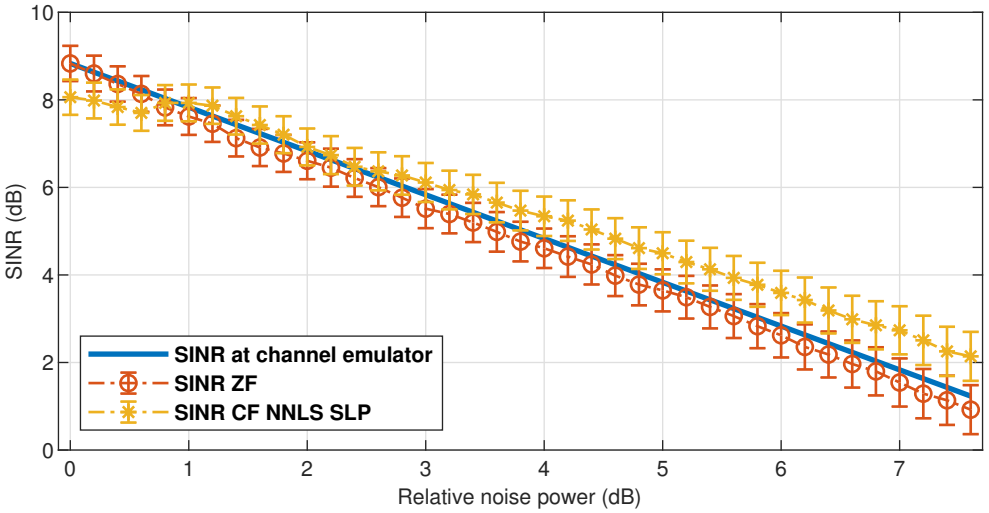

FIGURE 7. **Experimental SINR curves for the ZF and the SLP techniques and the channel emulator estimated SINR vs. the relative noise power.**

deviation of the average at each point by measuring the SINR from 1000 bundle frames. We also calculate the SINR value at the channel emulator as SINR_0 + relative noise power.

In Fig. 7 we can see the estimated and the expected SINR curves. In the ZF case, the SINR estimation is close to the SINR, calculated using the relative noise power at the channel emulator. The values are within the range of the standard deviation from the actual SINR. In the SLP case, the estimation of the SINR in the high SINR region (> 8 dB) is lower than the channel emulator SINR and SINR estimated for the ZF case. Below the 8 dB threshold, the SINR estimated for the SLP case is consistently higher than the actual SINR at the channel emulator. In the interference-limited region, the SLP-modified pilots greatly increase $\mathrm{P_r}$ in (11) but since only some pilots are changed SLP only partially increases $\mathrm{P_s}$ in (10). As a result, SNORE overestimates the noise variance of the signal. In the noise-limited region, the SLP-modified pilots do not contribute to the perceived $\mathrm{P_r}$, but still $\mathrm{P_s}$ is increased due to signal correlation properties. This leads to over-optimistic SINR estimations.

E. CODED BIT ERROR RATE PERFORMANCE OF CF NNLS SLP

In Fig. 8 we show the LDPC BER score using the QPSK signal at the UT 5. Each measurement point is an average of 1 million LDPC frames, where each block is 64800 bits long. The BER curves are plotted against the SINR estimated at the channel emulator, which is based on the noise power rather than the estimated SINR for the SLP or the ZF cases to achieve a fair comparison between the two techniques.

We can see that the SLP BER saturates (BER $= 1$) at lower SINR values than in the ZF case. The result is reproduced for every $\mathrm{C_R}$.

F. FRAME ERROR RATE PERFORMANCE OF CF NNLS SLP

In Fig. 9 we show the LDPC frame error rate using the QPSK signal at the UT 5. The total length of the LDPC frame with payload and parity check bits is 64800 bits. After the decoding process, the parity check bits are removed and the payload is transferred into the FER calculator. BCH (Bose-Chaudhuri-Hocquenghem) code is applied to correct the residual errors. Each measurement point is an average of 1 million frames. The FER curves are plotted against the channel emulator SINR as in the case of the BER benchmarks. We can see that the SLP FER saturates (FER $= 1$) at lower SINR values than in the ZF case. The result is reproduced for every $\mathrm{C_R}$.

G. SPECTRAL EFFICIENCY OF CF NNLS SLP

Spectral efficiency can be expressed as:

$$\mathrm{SE} = \frac{\mathrm{R_b}}{\mathrm{B_w}}(1 - \mathrm{FER})\left(\frac{\mathrm{bits/s}}{\mathrm{Hz}}\right), \tag{14}$$

where the payload bit rate is:

$$\mathrm{R_b} = \log_2(\mathrm{M})\mathrm{R_s}\mathrm{C_R}(\mathrm{bits/s}), \tag{15}$$

and the signal bandwidth is:

$$\mathrm{B_w} = \frac{1}{\mathrm{T_s}}(\beta + 1)(\mathrm{Hz}). \tag{16}$$

Given that the symbol period and the symbol rate are related as $\mathrm{T_s} = \frac{1}{\mathrm{R_s}}(\mathrm{s})$, $\mathrm{M} = 4$ for QPSK modulation order, and the matched filter roll-off factor is $\beta = 0.2$,

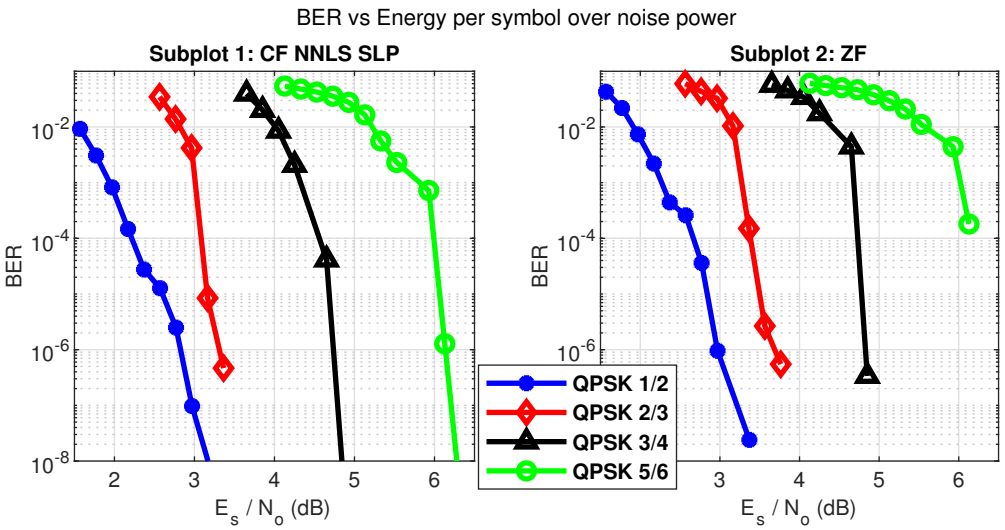

FIGURE 8. **LDPC BER plots for ZF and CF NNLS SLP vs the channel emulator SINR.**

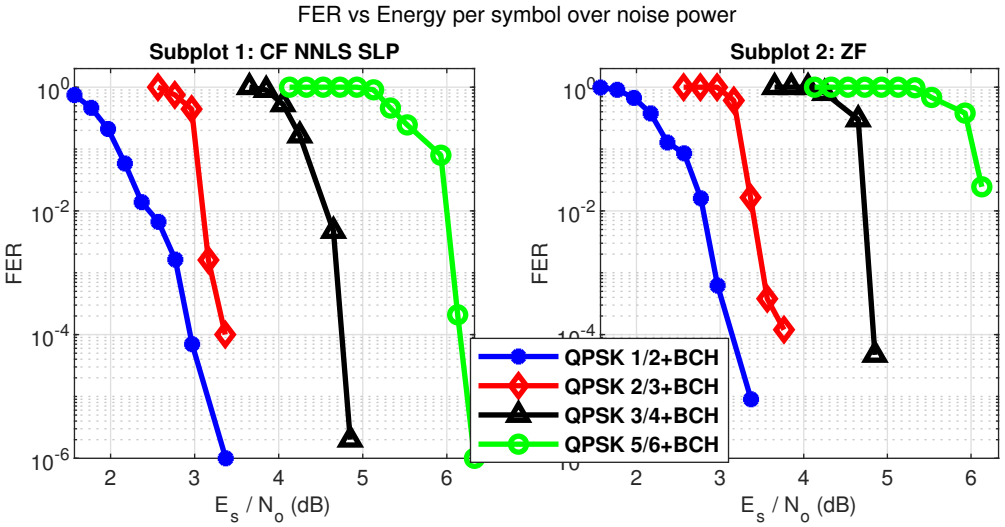

FIGURE 9. **LDPC FER plots for ZF and CF NNLS SLP vs expected SINR.**

we substitute eq. (15) and (16) back to eq. (14) and get the final expression for the spectral efficiency:

$$\mathrm{SE} = \frac{2\mathrm{C_R}}{(0.2+1)}(1-\mathrm{FER})\left(\frac{\mathrm{bits/s}}{\mathrm{Hz}}\right) \tag{17}$$

In Fig. 10 we can see the spectral efficiency of the ZF and the SLP techniques vs. the SINR. We can see that the SLP saturates at the maximum spectral efficiency at lower SINR values than the ZF. In the case of the $\mathrm{C_R}$ 1/2 the SLP achieves the maximum theoretical spectrum efficiency at 2.2 dB, for $\mathrm{C_R}$ 2/3 - 3.1 dB, $\mathrm{C_R}$ 3/4 - 4.5 dB, and $\mathrm{C_R}$ 5/6 - 6 dB. We can see that the SLP has a consistent advantage in the SE over the ZF. We can see that the SLP-modified symbols can be correctly decoded by the receiver with no prior knowledge of the modifications in the symbols of the conventional QPSK constellation. Additionally, these modified symbols result in lower BER and FER scores and improved spectrum efficiency.

IV. CONCLUSIONS

In this paper, we experimentally investigated that the SLP asymmetric symbols can be successfully decoded by the conventional receiver using the unmodified LLR and LDPC algorithms. We showed that the design of the receiver does not need special adjustments to correctly decode symbols when the transmitter uses the SLP technique to optimize the signal. We used the conventional LLR and LDPC decoder to extract the information bits from the symbols. Moreover, the SLP

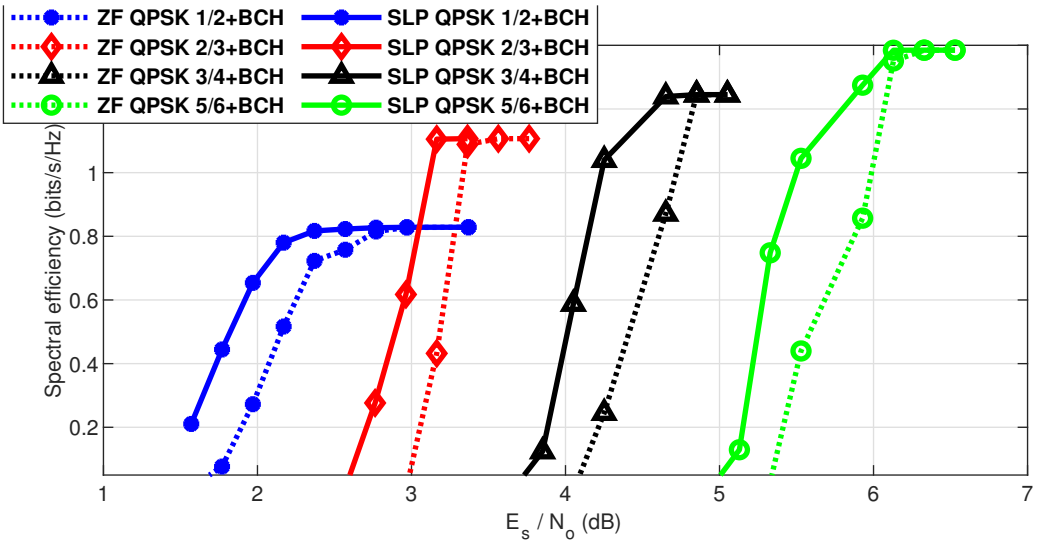

FIGURE 10. **Spectral efficiency plots for ZF and CF NNLS SLP vs expected SINR.**

showed improved received signal quality in terms of the SINR and Spectral efficiency compared to the linear precoding. However, we discovered that the SNORE algorithm tends to underestimate or overestimate the SINR values due to modified symbols by the SLP. The transmitter can disable the SLP while precoding the pilots to address this issue. Additionally, other types of modulated signals and SLP techniques can be verified using the presented setup in future works.

REFERENCES

[1] Kodheli, Oltjon and Lagunas, Eva and Maturo, Nicola and Sharma, Shree Krishna and Shankar, Bhavani and Montoya, Jesus Fabian Mendoza and Duncan, Juan Carlos Merlano and Spano, Danilo and Chatzinotas, Symeon and Kisseleff, Steven and Querol, Jorge and Lei, Lei and Vu, Thang X. and Goussetis, George, "Satellite Communications in the New Space Era: A Survey and Future Challenges," IEEE Communications Surveys & Tutorials, vol. 23, no. 1, pp. 70–109, 2021.

[2] Y. Ma and X. Li, "In-orbit Test Exploration for 5G NTN," in 2021 IEEE International Workshop on Electromagnetics: Applications and Student Innovation Competition (iWEM), vol. volume1, 2021, pp. 1–3.

[3] T. Heyn, A. Hofmann, S. Raghunandan, and L. Raschkowski, Non-Terrestrial Networks in 6G, 2022, pp. 101–116.

[4] A. Morello and V. Mignone, "DVB-S2X: the new extensions to the second generation DVB satellite standard DVB-S2," International Journal of Satellite Communications and Networking, vol. 34, no. 3, pp. 323–325, 2016. [Online]. Available: https://onlinelibrary.wiley.com/doi/abs/10.1002/sat.1167

[5] S. K. Sharma, S. Chatzinotas, and P.-D. Arapoglou, Satellite Communications in the 5G Era (Telecommunications). The Institution of Engineering and Technology, 2018.

[6] I. Ahmad, K. Nguyen, N. Letzepis, G. Lechner, and V. Joroughi, "Zero-Forcing Precoding with Partial CSI in Multi-beam High Throughput Satellite Systems," IEEE Transactions on Vehicular Technology, pp. 1–1, 2021.

[7] K. D. Pham, "A Control-Theoretic Approach to Precoding for Multi-Cast Multi-Beam over Satellite," in 2020 IEEE Aerospace Conference, March 2020, pp. 1–11.

[8] S. Chatzinotas, B. Ottersten, and R. De Gaudenzi, Cooperative and Cognitive Satellite Systems, 1st ed. Orlando, FL, USA: Academic Press, Inc., 2015.

[9] L. M. Marrero, J. C. Merlano-Duncan, J. Querol, S. Kumar, J. Krivochiza, S. K. Sharma, S. Chatzinotas, A. Camps, and B. Ottersten, "Architectures and Synchronization Techniques for Distributed Satellite Systems: A Survey," IEEE Access, vol. 10, pp. 45 375–45 409, 2022.

[10] G. Taricco and A. Ginesi, "Precoding for Flexible High Throughput Satellites: Hot-Spot Scenario," IEEE Transactions on Broadcasting, vol. 65, no. 1, pp. 65–72, 2019.

[11] S. Kisseleff, E. Lagunas, J. Krivochiza, J. Querol, N. Maturo, L. M. Marrero, J. Merlano-Duncan, and S. Chatzinotas, "Centralized Gateway Concept for Precoded Multi-beam GEO Satellite Networks," in 2021 IEEE 94th Vehicular Technology Conference (VTC2021-Fall), 2021, pp. 1–6.

[12] J. Duncan, J. Krivochiza, S. Andrenacci, S. Chatzinotas, and B. Ottersten, "Hardware Demonstration of Precoded Communications in Multi-Beam UHTS Systems," in 36th International Communications Satellite Systems Conference (ICSSC), Oct 2018.

[13] J. Duncan, J. Querol, N. Maturo, J. Krivochiza, D. Spano, N. Saba, L. Marrero, S. Chatzinotas, and B. Ottersten, "Hardware Precoding Demonstration in Multi-Beam UHTS Communications under Realistic Payload Characteristics," in 37th International Communications Satellite Systems Conference (ICSSC 2019), 2019.

[14] N. Maturo, J. C. M. Duncan, J. Krivochiza, J. Querol, D. Spano, S. Chatzinotas, and B. Ottersten, "Demonstrator of Precoding Technique for a Multi-Beams Satellite System," in 2019 8th International Workshop on Tracking, Telemetry and Command Systems for Space Applications (TTC), Darmstadt, Germany, Sep. 2019, pp. 1–8.

[15] B. Hamet, T. Kolb, C. Rohde, F. Leschka, M. U. Pavan Bhave and, and A. Lidde, "Over-the-Air Operation of Mobile and Multicast Linear Precoding for a Multi-Spot-Beam Mobile Satellite Service," in 24th Ka and Broadband Communications Conference, Oct 2018.

[16] B. Hamet, C. Rohde, P. Bhave, and A. Liddell, "Over-the-air Field Trials of Linear Precoding for Multi-spot-beam Satellite Systems," in 22th Ka and Broadband Communications Conference, Oct 2016.

[17] K. Storek, R. T. Schwarz, and A. Knopp, "Multi-Satellite Multi-User MIMO Precoding: Testbed and Field Trial," in ICC 2020 - 2020 IEEE International Conference on Communications (ICC), June 2020, pp. 1–7.

[18] J. Krivochiza, J. C. M. Duncan, J. Querol, N. Maturo, L. M. Marrero, S. Andrenacci, J. Krause, and S. Chatzinotas,

"End-to-end Precoding Validation over a Live GEO Satellite Forward Link," IEEE Access, pp. 1–1, 2021.

[19] C. B. Peel, B. M. Hochwald, and A. L. Swindlehurst, "A Vector-Perturbation Technique for Near-capacity Multi-antenna Multiuser Communication Part I: Channel Inversion and Regularization," IEEE Transactions on Communications, vol. 53, no. 1, pp. 195–202, Jan 2005.

[20] E. Björnson, M. Bengtsson, and B. E. Ottersten, "Optimal Multiuser Transmit Beamforming: A Difficult Problem with a Simple Solution Structure," CoRR, vol. abs/1404.0408, 2014. [Online]. Available: http://arxiv.org/abs/1404.0408

[21] M. Alodeh, D. Spano, A. Kalantari, C. G. Tsinos, D. Christopoulos, S. Chatzinotas, and B. Ottersten, "Symbol-Level and Multicast Precoding for Multiuser Multiantenna Downlink: A State-of-the-Art, Classification, and Challenges," IEEE Communications Surveys Tutorials, vol. 20, no. 3, pp. 1733–1757, thirdquarter 2018.

[22] J. Krivochiza, J. Merlano Duncan, S. Andrenacci, S. Chatzinotas, and B. Ottersten, "FPGA Acceleration for Computationally Efficient Symbol-Level Precoding in Multi-User Multi-Antenna Communication Systems," IEEE Access, vol. 7, pp. 15 509–15 520, 2019.

[23] J. Krivochiza, "End-to-end Signal Processing Algorithms for Precoded Satellite Communications," PhD dissertation, University of Luxembourg, Luxembourg, 2020.

[24] R. Bro and S. De Jong, "A Fast Non-Negativity-Constrained Least Squares Algorithm," Journal of Chemometrics, vol. 11, no. 5, pp. 393–401, 1997.

[25] J. Krivochiza, J. C. Merlano-Duncan, S. Andrenacci, S. Chatzinotas, and B. Ottersten, "Closed-Form Solution for Computationally Efficient Symbol-Level Precoding," in 2018 IEEE Global Communications Conference (GLOBECOM), Dec 2018.

[26] ETSI EN 302 307-2, "Digital Video Broadcasting (DVB); Second Generation Framing structure, Channel Coding and Modulation Systems for Broadcasting, Interactive Services, News Gathering and Other Broadband Satellite Applications; Part 2: DVB-S2 Extensions (DVB-S2X)," 2015.

[27] M. Alodeh, S. Chatzinotas, and B. Ottersten, "Symbol-Level Multiuser MISO Precoding for Multi-Level Adaptive Modulation," IEEE Transactions on Wireless Communications, vol. 16, no. 8, pp. 5511–5524, Aug 2017.

[28] ETSI TS 102 376-1, "Digital Video Broadcasting (DVB); Implementation Guidelines for the Second Generation System for Broadcasting, Interactive Services, News Gathering and Other Broadband Satellite Applications; Part 1: DVB-S2," 2015.

[29] N. E. Maammar, S. Bri, and J. Foshi, "Layered Offset Min-Sum Decoding for Low Density Parity Check Codes," in 2018 International Symposium on Advanced Electrical and Communication Technologies (ISAECT), Nov 2018, pp. 1–5.

[30] J. Duncan, J. Querol, N. Maturo, J. Krivochiza, D. Spano, N. Saba, L. Marrero, S. Chatzinotas, and B. Ottersten, "Hardware Precoding Demonstration in Multibeam UHTS Communications under Realistic Payload Characteristics," in Advances in Communications Satellite Systems. Proceedings of the 37th International Communications Satellite Systems Conference (ICSSC-2019), 2019, pp. 1–17.

JEVGENIJ KRIVOCHIZA (Member, IEEE) received the B.Sc. and M.Sc. degrees in electronic engineering in telecommunications physics and electronics from the Faculty of Physics, Vilnius University, in 2011 and 2013, respectively. He received his Ph.D. degree in electrical engineering from the Interdisciplinary Centre for Security, Reliability, and Trust (SnT), University of Luxembourg, in 2020. Currently, he is a Research Associate at SNT, University of Luxembourg. His main research topics are coming from development for FPGA silicon, software-defined radios, digital signal processing, precoding, interference mitigation, DVB-S2X, DVB-S2, and LTE systems. He works on DSP algorithms for SDR platforms for advanced precoding and beamforming techniques in next-generation satellite communications.

JUAN CARLOS MERLANO DUNCAN (Senior Member, IEEE) received the Diploma degree in electrical engineering from the Universidad del Norte, Barranquilla, Colombia, in 2004, the M.Sc. and Ph.D. Diploma (Cum Laude) degrees from the Universitat Politècnica de Catalunya (UPC), Barcelona, Spain, in 2009 and 2012, respectively. His research interests are wireless communications, remote sensing, distributed systems, frequency distribution and carrier synchronization systems, software-defined radios, and embedded systems. At UPC, he was responsible for the design and implementation of a radar system known as SABRINA, which was the first ground-based bistatic radar receiver using spaceborne platforms, such as ERS-2, ENVISAT, and TerraSAR-X as opportunity transmitters (C and X bands). He was also in charge of the implementation of a ground-based array of transmitters, which was able to monitor land subsidence with sub-wavelength precision. These two implementations involved FPGA design, embedded programming, and analog RF/Microwave design. In 2013, he joined the Institute National de la Recherche Scientifique, Montreal, Canada, as a Research Assistant in the design and implementation of cognitive radio networks employing software development and FPGA programming. He joined the University of Luxembourg in 2016, where he works as a Research Scientist in the COMMLAB laboratory working on SDR implementation of satellite and terrestrial communication systems.

JORGE QUEROL (Member, IEEE) was born in Forcall, Castelló, Spain, in 1987. He received the B.Sc. (+5) degree in telecommunication engineering, the M.Sc. degree in electronics engineering, the M.Sc. degree in photonics, and the Ph.D. degree (Cum Laude) in signal processing and communications from the Universitat Politècnica de Catalunya - BarcelonaTech (UPC), Barcelona, Spain, in 2011, 2012, 2013, and 2018, respectively. His Ph.D. thesis was devoted to the development of novel antijamming and counter-interference systems for Global Navigation Satellite Systems (GNSS), GNSS-Reflectometry, and microwave radiometry. One of his outstanding achievements was the development of a real-time standalone precorrelation mitigation system for GNSS, named FENIX, in a customized SDR platform. FENIX was patented, licensed, and commercialized by MITIC Solutions, a UPC spin-off company. Since 2018, he is a Research Associate with the SIGCOM research group of the Interdisciplinary Centre for Security, Reliability, and Trust (SnT) of the University of Luxembourg, Luxembourg. He is involved in several ESA and Luxembourgish national research projects dealing with signal processing and satellite communications. His research interests include SDR, real-time signal processing, satellite communications, 5G nonterrestrial networks, satellite navigation, and remote sensing. Dr. Querol was the Recipient of the Best Academic Record Award of the Year in Electronics Engineering at UPC in 2012, the First Prize of the European Satellite Navigation Competition Barcelona Challenge from the European GNSS Agency in 2015, the Best Innovative Project of the Market Assessment Program of EADA Business School in 2016, the award Isabel P. Trabal from Fundació Caixa d'Enginyers for its quality research during his Ph.D. in 2017, and the Best Ph.D. Thesis Award in remote sensing in Spain from the IEEE Geoscience and Remote Sensing Spanish Chapter in 2019.

SYMEON CHATZINOTAS (S'06–M'09–SM'13) is currently Full Professor / Chief Scientist I and Co-Head of the SIGCOM Research Group at SnT, University of Luxembourg. In the past, he has been a Visiting Professor at the University of Parma, Italy and he was involved in numerous Research and Development projects for the National Center for Scientific Research Demokritos, the Center of Research and Technology Hellas and the Center of Communication Systems Research, University of Surrey. He received the M.Eng. degree in telecommunications from the Aristotle University of Thessaloniki, Thessaloniki, Greece, in 2003, and the M.Sc. and Ph.D. degrees in electronic engineering from the University of Surrey, Surrey, U.K., in 2006 and 2009, respectively. He was a co-recipient of the 2014 IEEE Distinguished Contributions to Satellite Communications Award, the CROWNCOM 2015 Best Paper Award, and the 2018 EURASIC JWCN Best Paper Award. He has (co-)authored more than 400 technical papers in refereed international journals, conferences, and scientific books. He is currently on the editorial board of the IEEE Open Journal of Vehicular Technology and the International Journal of Satellite Communications and Networking.